RSC Advances

This article can be cited before page numbers have been issued, to do this please use: S. Ma, J. Feng, W. Qin, Y. Ju and X. Chen, *RSC Adv.*, 2015, DOI: 10.1039/C5RA09114D.

View Article Online
DOI: 10.1039/C5RA09114D

$CuFe_2O_4$@PDA Magnetic Nanomaterials with Core-shell Structure: Synthesis and Catalytic Application in Degradation of Methylene Blue in Water Solution

Su-dai Ma [a,b], Jie Feng [a,b], Wen-jie Qin [a,b], Yu-yun Ju [a,b], Xing-guo Chen [a, b, c, *]

[a] *State Key Laboratory of Applied Organic Chemistry, Lanzhou University, Lanzhou, 730000, China*

[b] *Department of Chemistry, Lanzhou University, Lanzhou, 730000, China*

[c] *Key Laboratory of Nonferrous Metal Chemistry and Resources Utilization of Gansu Province, Lanzhou University, Lanzhou, 730000, China*

[*] Corresponding author. Fax: +86-931-8912582 TEL: +86-931-8912763.
E-mail address: chenxg@lzu.edu.cn.

View Article Online
DOI: 10.1039/C5RA09114D

Abstract

In this paper, core-shell polydopamine (PDA)-encapsulated $CuFe_2O_4$ ($CuFe_2O_4$@PDA) magnetic nanoparticles (MNPs) were synthesized through in situ self-polymerization for the first time. The size of the core-shell product can be controlled by tuning the dopamine monomer concentration. The formation of PDA layer effectively enhanced the catalytic performance and provided a large specific surface area which offered more active sites for the effective interaction. The as-synthesized $CuFe_2O_4$@PDA MNPs were characterized and their catalytic activity was evaluated using the degradation of methylene blue (MB) in the presence of H_2O_2 as a model reaction. The experimental results showed that MB could be degraded efficiently using $CuFe_2O_4$@PDA MNPs as catalyst. Under the optimized conditions, the degradation efficiency of MB was above 97%. Furthermore, a possible reaction mechanism was discussed. Finally, the catalyst was used for effective degradation of MB in Yellow River water sample, which indicated its potential for practical applications in water pollutant removal and environmental remediation.

Keywords: Core-shell structure, $CuFe_2O_4$@PDA, Magnetic nanomaterial, Catalytic degradation, Methylene blue

View Article Online
DOI: 10.1039/C5RA09114D

1. Introduction

Rapid industrialization has led to an increased amount of discharged wastewater containing pollutant. Water pollution by organic dyes has become a serious environmental issue and received remarkable attention. The undesirable and immoderate release of wastewater containing organic dyes caused a pernicious impact, including destroying the balance of ecological system, destruction of the food chain existing in water ecosystem and endangering the animals and human beings,[1-5] etc. MB is an important member of the thiazine class of dyes. It is most widely used in paper, textiles, plastics, food, leather and cosmetic to color products.[6] However, acute exposure to MB will cause increased heart rate, shock, vomiting, Heinz body formation, jaundice, cyanosis, quadriplegia and tissue necrosis in humans.[7-10] The development of a process for the efficient treatment of MB-polluted wastewater is therefore of utmost importance. The various conventional treatment methods, such as physical adsorption,[11, 12] chemical oxidation,[13, 14] biological degradation,[15] photocatalytic degradation,[16, 17] and sonochemical technology[18] have been developed for the removal of such contaminants in wastewater. However, they suffer from some disadvantages including incomplete removal, additional equipment and disposal problem of sludge, etc. So it is still of great significance to discover a relatively low cost, easy operation and higher activity materials for efficient removal of organic dyes.

In recent years, the core-shell nanomaterials were developed as novel

View Article Online
DOI: 10.1039/C5RA09114D

nanostructured catalyst to remove organic dyes. The core-shell structural particles showed some special properties such as large specific surface area, adjustable size and devisable chemical composition. Moreover, the core-shell structural particles which may combine the advantages of "core" and "shell" showed enhanced physical and chemical properties in optics, electronics, magnetics and catalysis.[19-22] Thus, a lot of researches have been reported on the functional shells, including polymers, ligands, oxides or metals.[23, 24] Dopamine (DA), one of the important natural chemical neurotransmitters presented in various animals. It had the ability of adhering to almost all material surfaces to form thin and surface-adherent polydopamine (PDA) coating under mild condition.[25-28] In addition, compared with other shell such as SiO_2, Au, PDA shell displays the following characteristics: (1) the process of preparing a PDA coating seems to be simple, quick and 'green';[29, 30] (2) a robust interfacial binding force between the coating and the substrate through covalent bonds or other strong intermolecular interactions is easily adapted for a variety of materials without surface pretreatment; (3) PDA coating has plenty of functional groups such as amino and hydroxyl groups as well as π-π bonds, thus establishing further multiple modification.[31-34] (4) the good electrochemical behavior of a PDA coating with π-π stacking interaction can accelerate the electron transfer. On the basis of excellent characteristics, PDA coating is an outstanding candidate to develop core-shell nanomaterials.

However, the application of some nanomaterials was restricted due to difficult separation. This reason made it challenging to recycle and reuse the nanomaterials

View Article Online
DOI: 10.1039/C5RA09114D

efficiently, further affecting their decontamination efficiencies in dye removal. It is therefore crucial to look for stable, separated easily, and high catalytic activity nanomaterials from the viewpoint of practical application. The integration of PDA with superparamagnetic materials to form uniform core-shell nanocomposite particles has emerged as a viable solution. As an important kind of magnetic materials, copper ferrites ($CuFe_2O_4$) with good superparamagnetic nature as a magnetic core can make the catalysts efficiently separated from the reaction mixture with an external magnet, which prevents the loss of catalyst and renders the catalyst cost effective. Furthermore, $CuFe_2O_4$ nanoparticles possess excellent catalytic activity in various catalytic applications.[35-39]

As far as we know, the research on nanocompounds combining the advantages of the $CuFe_2O_4$ and PDA has not been reported. Hence, a facile and eco-friendly method for the fabrication of magnetically recyclable $CuFe_2O_4$@PDA MNPs with core-shell nanostructures was reported (Fig. 1). The size of the core-shell product was finely controlled by tuning the DA monomer concentration to form varying shell thickness of the PDA layer. Then, the $CuFe_2O_4$@PDA MNPs were employed to investigate its catalytic potential in the degradation of MB. Our results demonstrated that $CuFe_2O_4$@PDA MNPs possess excellent catalytic activity toward the degradation of MB, with advantages such as wide working pH range, environmentally friendly preparation, long-term stability and easily removed from the reaction system. It is expected to become a promising catalyst applied in water pollutant removal and environmental remediation.

View Article Online
DOI: 10.1039/C5RA09114D

2. Experimental

2.1. Materials

$FeCl_3 \cdot 6H_2O$ was purchased from Tianjin Shuangchuan Chemical Reagent Factory (Tianjin, China). Ethylene glycol and anhydrous ethanol were purchased from Tianjin Rionlon Bohua Pharmaceutical Chemical Co., Ltd. (Tianjin, China). Polyethylene glycol 20,000 was got from Xi'an Chemical Reagent Factory (Xi'an, China). Sodium acetate (NaAc), hydrochloric acid (HCl) and sodium hydroxide (NaOH) were got from Tianjin Guangfu Chemical Reagent Factory (Tianjin, China). 30% H_2O_2 (with extremely small amount of PO_4^{3-}) and MB were purchased from Tianjin Chemical Reagent Factory (Tianjin, China). $CuCl_2 \cdot 2H_2O$ and tris(hydroxymethyl)aminomethane (Tris) were obtained from Sinopharm Chemica Reagent Co. Ltd. Dopamine hydrochloride (DA) was obtained from Sigma Company. All chemicals were of analytical grade and used without any further purification. Ultrapure water was used throughout the whole experiment. The solution pH was adjusted using diluted HCl and NaOH solutions.

2.2. Preparation of $CuFe_2O_4$ magnetic nanoparticles

$CuFe_2O_4$ magnetic nanoparticles ($CuFe_2O_4$ MNPs) were prepared according to the literature procedures.[37] Briefly, $CuCl_2 \cdot 2H_2O$ (2.5 mmol) and $FeCl_3 \cdot 6H_2O$ (5 mmol) were dissolved in ethylene glycol (40 mL) to form a clear solution, followed by the addition of NaAc (3.6 g) and polyethylene glycol 20,000 (1.0 g). The mixture was

View Article Online
DOI: 10.1039/C5RA09114D

stirred vigorously for 30 min at 60~70℃ and then sealed in a teflon lined stainlesssteel autoclave (50 mL capacity). The autoclave was heated to and maintained at 200 ℃ for 8 h and allowed to cool to room temperature. The generated black $CuFe_2O_4$ MNPs were collected by magnetic separation, washed several times with ethanol and ultrapure water. The resulting solids were dried at 60 ℃ for 3 h under vacuum.

2.3. Synthesis of $CuFe_2O_4$@PDA magnetic nanoparticles

To prepare $CuFe_2O_4$@PDA MNPs, 0.4 g of the as-prepared $CuFe_2O_4$ MNPs was dispersed in 200 mL of dopamine-Tris solution (0.5 mg mL^{-1}, pH=8.5, 10 mM Tris-HCl buffer), and allowed to proceed for 8 h under stirring at room temperature. The resultant product was separated and collected with a magnet, and then washed with ultrapure water three times and dried at 60 ℃ for 3 h under vacuum.

2.4. Apparatus and characterization

A Tecnai G^2F30 instrument was used to obtain the morphology and particle size of the $CuFe_2O_4$ MNPs and $CuFe_2O_4$@PDA MNPs. A Nicolet Nexus 670 Fourier transform infrared spectrometer (FT-IR) was used to demonstrate the chemical nature of the products in KBr pellets. An X-ray diffraction (XRD) pattern of $CuFe_2O_4$ MNPs were carried out with a X'pertpro Philips X-ray diffractometer with Cu Kα radiation (λ=1.54056 Å) and scanning in the 2θ range of 10-80°. The magnetic property of the nanoparticles was measured at room temperature with a vibration sample

View Article Online
DOI: 10.1039/C5RA09114D

magnetometer (VSM, Lakeshore cryotronics 730, USA). A TU-1901 double beam UV-Vis spectrophotometer (Beijing Purkine General Instrument Co. Ltd., China) was used to implement scan spectrum and measure the absorbance for analysis. Fluorescent measurements were carried out by a RF-5301PC fluorescence (FL) spectrophotometer with a 1-cm quartz cell (Shimadzu, Kyoto, Japan). Mass spectra were recorded on an Esquire 6000 Mass spectrometer (Bruker Daltonics, USA). Inorganic ions in solution were analyzed using an DIONEX ICS-1500 Ion Chromatography (DIONEX, USA). Zeta potential measurements of $CuFe_2O_4$@PDA MNPs were performed with a Malvern Nano-ZS apparatus.

2.5. Evaluation of catalytic performance

The degradation of MB in the presence of H_2O_2 was chosen as a model reaction to evaluate the catalytic properties of the as-prepared $CuFe_2O_4$@PDA MNPs. During the degradation, the reactor of 50 mL capacity was immersed into a thermostated shaker. For typical experimental runs, 4 mg freshly prepared $CuFe_2O_4$@PDA MNPs was dispersed into 18 mL aqueous solution of MB (1.0×10^{-5} mol L^{-1}). The degradation of MB was initiated by rapid adding 2 mL H_2O_2 (5 mol L^{-1}) to the reaction solution. After the mixed solution was shaken for 30 min, a strong magnet was deposited at the bottom of the conical flask, and the $CuFe_2O_4$@PDA MNPs were isolated from the solution. The MB concentrations remained the aqueous solutions were measured at λ_{max}=656 nm. In addition, the adsorption experiment was carried out under the same conditions just without H_2O_2. After oscillating 30 min, the change in absorbance of

View Article Online
DOI: 10.1039/C5RA09114D

the mixture was measured again. The adsorption efficiency and the degradation efficiency of MB in the $CuFe_2O_4$-H_2O_2/$CuFe_2O_4$@PDA MNPs system were calculated according to the equations:

$$\eta_1 = [(A_0 - A_1)/A_0] \times 100\%$$

$$\eta_2 = [(A_1 - A_2)/A_1] \times 100\%$$

Where η_1 and η_2 were the adsorption efficiency and the degradation efficiency of MB, respectively; A_0 was the absorbance value of original MB. A_1 and A_2 were the maximum absorbance values of reaction solution at absence and present of H_2O_2, respectively.

For reusability, the catalysts were collected and washed with ultrapure water after the catalytic reaction finished and the above catalytic process was repeated for several times until obvious inactivation was acquired. The control experiments were carried out under the same conditions without catalyst and/or H_2O_2.

Besides, a 3 mg portion of $CuFe_2O_4$@PDA MNPs were dispersed in 6 mL of ultrapure water and stored for a month to test the stability of the PDA layer in aqueous solution. A 3 mg portion of $CuFe_2O_4$@PDA MNPs were dispersed in 6 mL of hydrochloric acid solution at pH 2 and pH 3 for 24 h to test the acid stability of the sample.

The Yellow River water was chosen as a practical environmental water sample for investigation. Before use, the sample was centrifuged (13,000 rpm) and filtered through a 0.45-μm membrane to remove any suspended particles. Stock solution was prepared by dissolving MB in the water sample. The degradation experiment was

View Article Online
DOI: 10.1039/C5RA09114D

carried out under the same conditions and same operation.

3. Results and Discussion

3.1. Characterization of $CuFe_2O_4$ and $CuFe_2O_4$@PDA MNPs

XRD analysis was used to identify the crystal structure of the $CuFe_2O_4$ MNPs. As shown in Fig. S1, except some Cu impurity peaks, all peaks were indexed to be $CuFe_2O_4$ (JCPDS 77-0010). There were five obvious diffraction peak at 2θ values of 29.98°, 35.22°, 57.10°, 62.28° and 74.06°, corresponding to the (220), (311), (422), (511) and (440) crystal plane of the spinel structure with $CuFe_2O_4$ MNPs. The reason of existence of metallic copper was that the strong reducing capability of ethylene glycol used as solvent in the preparation of the $CuFe_2O_4$ MNPs.[40]

The morphology and size of the as-prepared $CuFe_2O_4$ MNPs and $CuFe_2O_4$@PDA MNPs were determined by TEM. Fig. 2a clearly displayed that the $CuFe_2O_4$ MNPs were spherical and dispersive with an average size of about 150±20 nm. As shown in Fig. 2b, a continuous layer, which exhibited a fine increment in brightness in comparison to the dark inner core, was clearly observed on the outer shell of the $CuFe_2O_4$ core. From Fig. 2a and 2b, it was very clear that the $CuFe_2O_4$@PDA MNPs were encapsulated with a typical core-shell structure. There was a clear interface between the PDA shell and the $CuFe_2O_4$ core, indicating a tight encapsulation. In this process, the size of the $CuFe_2O_4$@PDA particle can be easily controlled by tuning the DA monomer concentration. As shown in Fig. 3, when the size of the $CuFe_2O_4$ microspheres was fixed and the DA monomer concentration was changed from 0.5

View Article Online
DOI: 10.1039/C5RA09114D

mg mL^{-1} to 4 mg mL^{-1}, the average thickness of the PDA shell was 15 nm, 24 nm, 32 nm, 55 nm and 95 nm, respectively. The typical EDX pattern of $CuFe_2O_4$@PDA MNPs in Fig. 3f illustrated the fractions of all the elements in the MNPs. The appearance of N element indicated the successful modification of PDA on $CuFe_2O_4$ MNPs.

FT-IR was employed to examine the surface composition of the synthesized the $CuFe_2O_4$ and $CuFe_2O_4$@PDA MNPs. As shown in Fig. 4a, the absorption band at 596 cm^{-1} and 417 cm^{-1} were ascribed to stretching vibration of tetrahedral complexes and octahedral complexes, respectively. The metal ions in ferrite were situated in two different sublattices owing to the geometrical configuration of the oxygen nearest neighbors.[41] The adsorption peak at 3433 cm^{-1} represented the stretching mode of H_2O molecules and OH groups. The absorption peak at 1626 cm^{-1} on spectrum referred to the vibration of remainder H_2O in the sample.[37] In Fig. 4b there were several new peaks compared with $CuFe_2O_4$ MNPs. The new peak at 1487 cm^{-1} belonged to the C=C stretching vibrations of aromatic ring in the PDA polymer. The absorption peak at 1576 cm^{-1} was attributed to N–H stretching and 1298 cm^{-1} was assigned to the C–O stretching of phenolic hydroxyl group.[28, 42] The peak at 3433 cm^{-1} of $CuFe_2O_4$@PDA MNPs was broader than that of $CuFe_2O_4$ MNPs, resulting from the overlapping of hydroxyls, water adsorbed in PDA polymer and amines of PDA. The FT-IR spectrum indicated that the PDA was indeed coated on the surface of the $CuFe_2O_4$ MNPs and the main structure of $CuFe_2O_4$ was not changed by the modification.

View Article Online
DOI: 10.1039/C5RA09114D

Moreover, VSM measurement was employed to investigate the magnetic properties of the nanostructure. As shown in Figure 5, a hysteresis loop of typical $CuFe_2O_4$ and $CuFe_2O_4$@PDA MNPs measured by sweeping the external field between 1.5 and 1.0 T at room temperature. In the VSM magnetization curves of the $CuFe_2O_4$ and $CuFe_2O_4$@PDA MNPs, there were no hysteresis, and the remanence and coercivity were negligible, indicating the superparamagnetism of these nanomaterials. Although the saturation magnetization value of $CuFe_2O_4$@PDA MNPs (39.15 emu/g) was lower than $CuFe_2O_4$ MNPs (44.80 emu/g) due to the existence of non-magnetic PDA coating, the $CuFe_2O_4$@PDA MNPs were readily separated from solution with a magnet due to their superparamagnetism and large saturation magnetization. All the above results revealed the successful synthesis of the $CuFe_2O_4$@PDA MNPs.

3.2. Evaluation of catalytic performance

In order to investigate the catalytic activity of the $CuFe_2O_4$@PDA MNPs, MB was used as a typical dye pollutant in the removal of organic pollutants for wastewater treatments. The degradation curve of the MB was shown in Fig. 6 by measuring the change of the absorbance at 665 nm. It showed that after the addition of the $CuFe_2O_4$@PDA MNPs, the characteristic absorbance of MB at 665 nm nearly disappeared, and the solution became colorless. It indicated that the $CuFe_2O_4$@PDA MNPs exhibited excellent catalytic activity in the degradation of MB.

Moreover, the degradation efficiency of the $CuFe_2O_4$@PDA MNPs-H_2O_2 was 99% after 30 min (Fig. 7a), which was more effective than the $CuFe_2O_4$ MNPs-H_2O_2. The

View Article Online
DOI: 10.1039/C5RA09114D

catalytic performance of $CuFe_2O_4$@PDA MNPs was about 668% and 434% higher than that of $CuFe_2O_4$ MNPs at 2 min and 5 min, respectively (Fig. S2). However, no obvious decolorization was observed under the conditions of H_2O_2 only. The above results indicated that the core of the $CuFe_2O_4$ MNPs itself owned catalytic property. But the PDA layer can dramatically enhance the catalytic performance in MB degradation. The enhanced catalytic activity of $CuFe_2O_4$@PDA MNPs was probably caused by the synergistic effect between $CuFe_2O_4$ MNPs and PDA layer. In this process, MB was more easily absorbed on the surface of the $CuFe_2O_4$@PDA MNPs than $CuFe_2O_4$ MNPs.

In order to further verify the adsorption effect of PDA layer, the adsorptions experiment of $CuFe_2O_4$@PDA MNPs and $CuFe_2O_4$ MNPs were also studied (Fig. 7b). There were nearly no decolorization in the presence of $CuFe_2O_4$ MNPs after 30 min, which demonstrated the $CuFe_2O_4$ MNPs could not adsorb MB. However, in the $CuFe_2O_4$@PDA-MB system, MB could be removed about 40% in the same time. Consequently, in these two parallel tests, the significant discrepancy was mainly caused by adsorption capacity of PDA layer. It is noted that there were three aspects may contribute to the adsorption of PDA layers and MB: (a) because of the large amount of functional groups (amino and catechol groups) on the surface of PDA layer, π-π interaction and hydrogen bonding induced the adsorption of MB toward the PDA surface.[43-45] (b) the PDA layer also provided a large specific surface area and active sites for this process. (c) the electrostatic interactions favoured the efficient enrichment of the MB molecules on the PDA surfaces. To demonstrate this effect, the

View Article Online
DOI: 10.1039/C5RA09114D

zeta potential of $CuFe_2O_4$@PDA MNPs was determined to be negatively charged in a wide pH range (Fig. S3), suggesting strong electrostatic interactions with positively charged MB (Fig. S4). To further confirm the presence of electrostatic interactions, the influence of pH on the adsorption performance of $CuFe_2O_4$@PDA MNPs was investigated (Fig. S5). It was evident that MB was absorbed by the $CuFe_2O_4$@PDA MNPs faster at higher pH, which was most likely attributed to the stronger electrostatic interactions under higher pH. As confirmed by zeta potential measurement of $CuFe_2O_4$@PDA MNPs, the MNPs showed more negatively charged at higher pH. All of the evidences suggested that the PDA layer showed efficient adsorption of MB in addition to the high catalytic activity. As a result, the local concentration of MB at PDA surfaces was much higher than that in bulk solution. Therefore, the rate of the catalytic reaction and the performance of the catalysts were significantly improved.

3.3. Effect of operating parameters on MB degradation.

3.3.1. Effect of dopamine monomer concentration

To confirm the difference in catalytic performance of catalysts with different shell thickness, we made a comparison of MB degradation efficiency. As illustrated in Fig. 8a, the $CuFe_2O_4$@PDA MNPs showed a distinct increase in MB degradation efficiency compared to $CuFe_2O_4$ MNPs of which degradation efficiency is only 69.18%, clearly demonstrating that the $CuFe_2O_4$@PDA MNPs showed much higher catalytic activity. However, the degradation efficiency almost reached to the plateau

View Article Online
DOI: 10.1039/C5RA09114D

when the concentration of DA monomer was 0.5 mg mL^{-1} to 2 mg mL^{-1}. As the DA monomer concentration was more than 2 mg mL^{-1}, only slight decrease of degradation efficiency may be caused by the increase of PDA shell thickness. The PDA shell thickness was too thick, which would limit the catalytic activity of inner core $CuFe_2O_4$. Therefore, 0.5 mg mL^{-1} of DA monomer concentration (i.e., the $CuFe_2O_4$@PDA MNPs with 15 nm thickness of the PDA shell) was selected for further experiments.

3.3.2. Effect of the $CuFe_2O_4$@PDA MNPs amount

Fig. 8b illustrated the MB degradation in the $CuFe_2O_4$@PDA-H_2O_2 system with various loads of $CuFe_2O_4$@PDA MNPs. Compared with the H_2O_2 system (i.e., the zero load of $CuFe_2O_4$@PDA MNPs), the introduction of $CuFe_2O_4$@PDA MNPs significantly enhanced the degradation efficiency of MB. Because the $CuFe_2O_4$@PDA MNPs acted as catalyst to accelerate the decomposition of H_2O_2, the consequence of strong oxidizing radical species were easier generated. When the $CuFe_2O_4$@PDA MNPs amount range from 0 to 4 mg, the degradation efficiency of MB was greatly increased. While the amount of the $CuFe_2O_4$@PDA MNPs exceeded 4 mg, the degradation efficiency essentially achieved constant value. Hence, 4 mg was chose as optimal $CuFe_2O_4$@PDA MNPs amount.

3.3.3. Effect of H_2O_2 concentration

Fig. 8c gave the degradation efficiency of MB in the $CuFe_2O_4$@PDA-H_2O_2 system

View Article Online
DOI: 10.1039/C5RA09114D

with different concentrations of H_2O_2. As the H_2O_2 concentration increased to 0.5 mol L^{-1}, the degradation efficiency of MB increased rapidly. Nonetheless when the H_2O_2 concentration enhanced from 0.5 to 1.0 mol L^{-1}, the degradation efficiency reduced gradually. The degradation efficiency of MB reached a maximum when the H_2O_2 concentration was 0.5 mol L^{-1}. To our knowledge, H_2O_2 was not stable under high concentration. Considering the above factors, 0.5 mol L^{-1} of H_2O_2 was selected in subsequent experiments.

3.3.4. Effect of pH

The solution pH was a very important operation parameter in catalytic reaction. The effect of pH on the degradation efficiency of MB was researched in the range of 2-10. As can be seen from Fig. 8d, the MB degradation worked very effectively over a wide pH range from 4.0 to 10.0. It was very favorable to the practical treatment of wastewater because there was no need to adjust the pH of the solution. The degradation of MB would be very favorable to occur at pH 4.0 to pH 6.0; however, it was unlike the other typical reaction for MB degradation, which was usually performed at approximately pH 4.0.[46] This signified that the robust PDA layer could effectively protect the $CuFe_2O_4$ cores and the $CuFe_2O_4$@PDA MNPs could improve the pH tolerance. This work chose 6.0 as optimal pH value, because it was the most close to the pure water pH.

3.3.5. Effect of temperature and reaction time

View Article Online
DOI: 10.1039/C5RA09114D

Temperature played an important role in most chemical reactions. The influence of temperature on the degradation of MB was investigated between 298 K and 313 K. The extent of the degradation reaction of MB by time at different temperatures was plotted. Fig. S6 demonstrated that the degradation efficiency of MB was higher at higher temperatures within the tested temperature range. Furthermore, the reaction time needed for complete removal of MB dropped from 30 min to 15 min along with the temperature increasing from 298 K to 313 K. The effective interaction of reactant could be accelerated at high temperature, resulting in enhancement of reaction rate. Also, the catalytic activity of $CuFe_2O_4$@PDA MNPs kept unchanged even at a high-temperature (313 K). The results demonstrated the high-temperature tolerance of the $CuFe_2O_4$@PDA MNPs, which was impossible for some catalyst due to denaturation at higher temperatures. So in the treatment of wastewater, high temperature could be taken to accelerate the removal of pollutant. For operational convenience, a temperature of 303 K (room temperature) was selected for all the experiment. In addition, the complete degradation of MB took place in 30 min and the color of the reaction mixture solution changed from blue to colorless.

In summary, the optimized conditions for MB degradation using the $CuFe_2O_4$@PDA-H_2O_2 system were as follows: 4 mg $CuFe_2O_4$@PDA MNPs, 0.5 mol/L H_2O_2, pH 6.0, temperature 30 ℃, oscillation time 30 min. Under optimal conditions, the MB could be removed completely, and the degradation efficiency was above 97%.

3.4. The reusability and the stability of $CuFe_2O_4$@PDA MNPs

View Article Online
DOI: 10.1039/C5RA09114D

The reusability and stability of catalyst are crucial properties to evaluate the catalytic performance. Therefore, the reusability of the as-prepared $CuFe_2O_4$@PDA MNPs was explored by checking the cycle number dependence of MB degradation loading the same $CuFe_2O_4$@PDA MNPs. Then the $CuFe_2O_4$@PDA MNPs were carefully collected after each cycle and reversibly reused in the identical catalytic system. As shown in Fig. S7, the catalyst could be successfully recycled and reused for five successive cycles with a degradation efficiency of >85%.

Furthermore, as shown in Fig. S8a, after a month of soaking in aqueous solution, the PDA layers were still intact coated on the $CuFe_2O_4$ cores and the morphology remained unchanged. Even dispersed under a strong acid environment (pH 2 and pH 3) for over 24 h, the TEM images (Fig. S8b, c) showed that the $CuFe_2O_4$@PDA MNPs still maintained the distinct core-shell structure. It is indicated that the robust PDA layer could effectively protect the $CuFe_2O_4$ core under strong acid conditions and show good stability in aqueous environment over a reasonably long period of time. Therefore, the magnetically separable $CuFe_2O_4$@PDA MNPs have outstanding recyclable and stable performance. It is expected to be used for a promising efficient catalyst in wastewater treatment.

3.5. Kinetics of the degradation of MB

Fig. 9 showed the time-dependent UV-Vis spectra change of MB catalyzed with $CuFe_2O_4$@PDA MNPs. The absorbance peak at 665 nm gradually attenuated during the degradation process and finally disappeared. Furthermore, the degradation rate

View Article Online
DOI: 10.1039/C5RA09114D

was evaluated. For the MB degradation reaction, the ratio of the concentration c_t of MB at time t to its initial value c_0 at t= 0 were directly given by the ratio of the respective absorbance A_t/A_0 (A represents the absorbance at 665 nm). Because H_2O_2 was in excess ($c_{MB}/c_{H_2O_2} = 9/500000$) and its concentration was considered as a constant during the reaction process, the reaction kinetics could be treated as pseudo-first-order:

$$dc_t/dt = -k_{app}c_t$$

$$\text{or} \quad \ln(c_t/c_0) = \ln(A_t/A_0) = -k_{app}t$$

where the apparent rate constant k_{app} could be obtained from the plot of $\ln(A_t/A_0)$ versus the reaction time. Linear relationships between $\ln(A_t/A_0)$ and reaction time were obtained using $CuFe_2O_4$@PDA MNPs as catalyst, and the rate constant, k_{app} was calculated as 9.89×10^{-2} min^{-1} for the reaction.

Although the previous reported catalysts loading of gold or silver nanoparticles could also exhibit great catalytic activity for the reduction of MB,[43, 47] using expensive and scarce noble metals limited the widespread application of these catalysts.[48] By contrast, the $CuFe_2O_4$@PDA MNPs were low-cost and affordable. Furthermore, the $CuFe_2O_4$@PDA MNPs exhibited other advantages, such as the wider working pH range, long-term stability, operational stability and higher catalytic efficiency compared with the analogous catalysts.[18, 49, 50]

3.6. Possible reaction mechanism

According to the above discussions, the degradation mechanism of MB was

View Article Online
DOI: 10.1039/C5RA09114D

investigated and proposed. Obvious decolorization of MB was observed under the conditions of $CuFe_2O_4$@PDA MNPs and H_2O_2. In order to validate the reason of decolorization, the UV-vis spectra were first inspected. Fig. 10 showed that after the addition of the $CuFe_2O_4$@PDA MNPs, the adsorption peak of 665 nm and 291 nm, which respectively represented the characteristic adsorption of conjugated structure and substituent benzene of MB, both vanished; a new strong adsorption peak (λ= 251 nm), which represented the characteristic adsorption of aromatic structure of catalytic degradation product, appeared.[43, 44] It indicated that the destruction of the whole MB molecular or the chromophore of MB. In order to further determine intermediates and final products, solutions of the MB and the MB was catalyzed by $CuFe_2O_4$@PDA MNPs were analyzed using ESI-MS (Fig. S9 and S10). It is noteworthy that new fragments of m/z 228, 191, 131 were detected, demonstrating 3, 7-diamino-phenothiazine-5-ium, 2, 5-diaminobenzenesulfonic acid and dl-norleucine were formed in degradation process (Table S1). The generation pathways of these fresh intermediates were speculated,[51-53] as shown in Fig. S11. Most Cl^- may be ionized during the dissolution of MB and existed in the detached state. N−CH_3 with the lowest bond energy was first broken. Then C−S and C−N were broken, C−S transformed into C−SO_3H. C−NH_2 bond in the remaining structure was broken and C−SO_3H transformed into C−OH in the following degradation. The DL-Norleucine generated as the ring in 1-amino-3,4-dihydroxybenzene opened. Mass spectra data provided overwhelming evidence of the MB degradation, which was in accordance with the results of UV-Vis spectra. Additionally, the ion chromatography was used to

View Article Online
DOI: 10.1039/C5RA09114D

further determine ions in resultant degradation solution. As shown in Fig. S12, Cl^-, NO_2^-, NO_3^-, SO_4^{2-} were detected. The generation of NO_2^-, NO_3^- and SO_4^{2-} further manifested C-S and C-N bond gradually cleavage in the degradation process.[52, 53] These overall results confirmed that decolorization of MB was due to the MB was degraded by $CuFe_2O_4$@PDA MNPs as a catalyst in the presence of H_2O_2.

Based on the intermediate and final products detected, the degradation mechanism for MB is analyzed and described, as shown in Fig. S13. The MB degradation in $CuFe_2O_4$@PDA-H_2O_2 system was mainly due to the synergistic effect of the $CuFe_2O_4$ core catalysis and PDA shell adsorption capacity. When the $CuFe_2O_4$@PDA MNPs were added and used for catalysis, H_2O_2 molecules and MB were adsorbed on the surface of $CuFe_2O_4$@PDA MNPs. The surface-adsorbed H_2O_2 molecules were activated to generate the ·OH, which further react with adsorbed MB to initiate the degradation and/or diffuse into the solution to attack MB molecules near the $CuFe_2O_4$@PDA/solution interface. Furthermore, the PDA layer with π-π stacking interaction and the $CuFe_2O_4$ core with 'd^n' (n= 5-9) electronic configuration could accelerate the electron transfer.[37, 54] The faster electron transferred on catalyst surface, the faster the reaction processed. To evidence this assumption, a fluorescence technique was used to detect of the produced ·OH radicals by adding the fluorescent probe terephthalic acid into the $CuFe_2O_4$@PDA-H_2O_2 system, where terephthalic acid could easily react with ·OH to yield a strongly fluorescent product 2-hydroxy terephthalic acid.[55, 56] It was clearly shown in Fig. S14 that fluorescence intensity enhanced gradually with the increasing concentration of the $CuFe_2O_4$@PDA MNPs,

View Article Online
DOI: 10.1039/C5RA09114D

which suggested that the amount of generated ·OH increased as $CuFe_2O_4$@PDA MNPs increased. However, no fluorescence intensity was observed in the absence of H_2O_2. All of the above results indicated that H_2O_2 molecules were adsorbed on the surface of the $CuFe_2O_4$@PDA MNPs and then activated by the $CuFe_2O_4$@PDA MNPs to generate reactive oxygen species. All the evidences suggested that the synergistic mechanism was feasible.

3.7. The application

Finally, in order to verify whether the nanocomposite could be applied to environmental water, the Yellow River water in Lanzhou section was collected and used as a practical sample. The Yellow River water formed a blue solution after being spiked with MB as a pollutant. Then 4 mg of the $CuFe_2O_4$@PDA MNPs was added to this water in the presence of H_2O_2. Satisfactory results were obtained that the solution became colorless, and the degradation efficiency was still above 97%. The $CuFe_2O_4$@PDA MNPs were then easily separated by a magnet and could be reused for further reactions. Therefore, the $CuFe_2O_4$@PDA MNPs were successfully used as a catalyst for the degradation of MB for complex environmental water samples and the proposed method was reliable.

4. Conclusions

In summary, a simple method to prepare polydopamine modified $CuFe_2O_4$ MNPs was proposed. The PDA was directly grafted onto the $CuFe_2O_4$ using one step

View Article Online
DOI: 10.1039/C5RA09114D

self-polymerization reaction to form well-defined core-shell nanostructures. The $CuFe_2O_4$@PDA MNPs exhibited excellent catalytic activity for the degradation of MB in the presence of H_2O_2. The $CuFe_2O_4$@PDA MNPs could be easily separated by a magnet after the catalytic reaction. In addition, the significant synergistic effect of the $CuFe_2O_4$ core catalysis and PDA shell adsorption capacity was observed. MB and H_2O_2 could be absorbed on the surface of the $CuFe_2O_4$@PDA MNPs. The surface-adsorbed H_2O_2 molecules were activated to generate the ·OH, then it further reacted with adsorbed MB to initiate the degradation. The formation of PDA layer effectively enhanced the catalytic performance and protected the $CuFe_2O_4$ core to improve the stability. The versatile PDA polymer coating on the $CuFe_2O_4$ core also allowed the further surface functionalization for the development of multifunctional nanomaterials. Because of its merits such as wide working pH range, simple preparation, long-term stability, good recyclability and high catalytic performance, the $CuFe_2O_4$@PDA MNPs as potential catalysts will be facilitated to apply in various fields such as environmental protection, bioseparator, biosensor, and so on.

Acknowledgements

The authors are grateful for financial support from the National Natural Science Foundation of China (No. 21375053) and Special Doctorial Program Fund from the Ministry of Education of China (No. 20130211110039).

View Article Online
DOI: 10.1039/C5RA09114D

References

1 T. Warang, N. Patel, R. Fernandes and N. Bazzanella, *Appl. Catal. B: Environ.*, 2013, **132**, 204-211.

2 V. Vimonses, B. Jin and C. W. Chow, *J. Hazard. Mater.*, 2010, **177,** 420-427.

3 M. Doğan, H. Abak and M. Alkan, *J. Hazard. Mater.*, 2009, **164,** 172-181.

4 B. S. Kaith, J. Dhiman and J. K. Bhatia, *RSC Adv.*, 2015, **5,** 39771-39784.

5 Y. Y. Lau, Y. S. Wong, T. T. Teng, N. Morad, M. Rafatullah and S. A. Ong, *RSC Adv.*, 2015, **5,** 34206-34215.

6 L. J. Yang, Y. Y. Zhang, X. Y. Liu, X. Q. Jiang, Z. Z. Zhang, T. T. Zhang and L. Zhang, *Chem. Eng. J.*, 2014, **246,** 88-96.

7 M. T. Uddin, M. A. Islam, S. Mahmud and M. Rukanuzzaman, *J. Hazard. Mater.*, 2009, **164,** 53-60.

8 M. Rafatullah, O. Sulaiman, R. Hashim and A. Ahmad, *J. Hazard. Mater.*, 2010, **177,** 70-80.

9 L. Li, X. L. Liu, M. Gao, W. Hong, G. Z. Liu, L. Fan, B. Hu, Q. H. Xia, L. Liu, G. W. Song and Z. S. Xu, *J. Mater. Chem.*, 2014, **A 2,** 1795-1801.

10 H. T. Wang, H. Y. Ma, W. Zheng, D. D. An and C. Z. Na, *Appl. Mater. Interfaces,* 2014, **6,** 9426-9434.

11 V. J. Vilar, C. Botelho and R. A. Boaventura, *J. Hazard. Mater.*, 2007, **147,** 120-132.

12 D. Özer, G. Dursun and A. Özer, *J. Hazard. Mater.*, 2007, **144,** 171-179.

13 L. Yue, K. H. Wang, J. B. Guo, J. L. Yang, X. Luo, J. Lian and L. Wang, *J. Ind. Eng. Chem.*, 2014, **20,** 725-731.

14 R. Prihod'ko, I. Stolyarova, G. Gündüz, O. Taran, S. Yashnik, V. Parmon and V. Goncharuk, *Appl. Catal. B: Environ.*, 2011, **104,** 201-210.

View Article Online
DOI: 10.1039/C5RA09114D

15 O. Olukanni, A. Osuntoki, D. Kalyani, G. Gbenle and S. Govindwar, *J. Hazard. Mater.*, 2010, **184,** 290-298.

16 M. Wu, J. Liu, J. Jin, C. Wang, S. Z. Huang, Z. Deng, Y. Li and B. L. Su, *Appl. Catal. B: Environ.*, 2014, **150,** 411-420.

17 Y. C. Hsiao, T. F. Wu, Y. S. Wang, C. C. Hu and C. Huang, *Appl. Catal. B: Environ.*, 2014, **148,** 250-257.

18 N. Wang, L. H. Zhu, D. L. Wang, M. Q. Wang, Z. F. Lin and H. Q. Tang, *Ultrason. Sonochem.*, 2010, **17,** 526-533.

19 F. Caruso, X. Shi, R. Caruso and A. Susha, *Adv. Mater.*, 2001, **13,** 740-744.

20 S. M. Marinakos, J. P. Novak, L. C. Brousseau, A. B. House, E. M. Edeki, J. C. Feldhaus and D. L. Feldheim, *J. Am. Chem. Soc.*, 1999, **121,** 8518-8522.

21 Y. Lu, Y. D. Yin, B. T. Mayers and Y. Xia, *Nano Lett.*, 2002, **2,** 183-186.

22 P. Tartaj and C. J. Serna, *J. Am. Chem. Soc.*, 2003, **125,** 15754-15755.

23 L. Y. Hao, C. L. Zhu, W. Q. Jiang, C. N. Chen, Y. Hu and Z. Y. Chen, *J. Mater. Chem.*, 2004, **14,** 2929-2934.

24 Z. M. Liu, Y. L. Liu, H. F. Yang, Y. Yang, G. L. Shen and R. Q. Yu, *Anal. Chim. Acta*, 2005, **533,** 3-9.

25 H. Lee, S. M. Dellatore, W. M. Miller and P. B. Messersmith, *Science*, 2007, **318,** 426-430.

26 Q. Ye, F. Zhou and W. M. Liu, *Chem. Soc. Rev.*, 2011, **40,** 4244-4258.

27 B. Fei, B. T. Qian, Z. Y. Yang, R. H. Wang, W. C. Liu, C. L. Mak and John H. Xin, *Carbon*, 2008, **46,** 1795-1797.

28 T. Zeng, X. L. Zhang, H. Y. Niu, Y. R. Ma, W. H. Li and Y. Q. Cai, *Appl. Catal. B: Environ.*, 2013,

View Article Online
DOI: 10.1039/C5RA09114D

134, 26-33.

29 H. Lee, Y. Lee, A. R. Statz, J. Rho, T. G. Park and P. B. Messersmith, *Adv. Mater.*, 2008, **20,** 1619-1623.

30 Y. Y. Li, C. Qin, C. Chen, Y. C. Fu, M. Ma and Q. J. Xie, *Actuat. B: Chem.*, 2012, **168,** 46-53.

31 W. Zhang, Y. Tang, J. Liu, Y. J. Ma, L. Jiang, W. Huang, F. W. Huo and D. B. Tian, *J. Mater. Chem. B*, 2014, **2,** 8490-8495.

32 Y. F. Wei, J. H. Kong, L. P. Yang, L. Ke, H. R. Tan, H. Liu, Y. Z. Huang, X. W. Sun, X. H. Lu and H. J. Du, *J. Mater. Chem. A*, 2013, **1,** 5045-5052.

33 M. Mart´ın, P. Salazar, R. Villalonga, S. Campuzano, J. M. Pingarr´on and J. L. Gonz´alez-Mora, *J. Mater. Chem. B*, 2014, **2,** 739-746.

34 N. Y. Wang, Y. Liu, Z. W. Qiao, L. Diestel, J. Zhou, A. Huang and J. Caro, *J. Mater. Chem. A*, 2015, **3,** 4722-4728.

35 Y. B. Wang, H. Y. Zhao, M. F. Li, J. Q. Fan and G. H. Zhao, *Appl. Catal. B: Environ.*, 2014, **147,** 534-545.

36 Z. H. Chonco, L. Lodya, M. Claeys and E. van Steen, *J. Catal.*, 2013, **308,** 363-373.

37 J. Feng, L. Su, Y. H. Ma, C. L. Ren, Q. Guo and X. G. Chen, *Chem. Eng. J.*, 2013, **221,** 16-24.

38 D. Kundu, N. Mukherjee and B. C. Ranu, *RSC Adv.*, 2013, **3,** 117-125.

39 S. M. Baghbanian and M. Farhang, *RSC Adv.*, 2014, **4,** 11624-11633.

40 H. Deng, H. Y. Chen and H. Li, *Mater. Chem. Phys.*, 2007, **101,** 509-513.

41 R. K. Selvan, C. Augustin, L. J. Berchmans and R. Saraswathi, *Mater. Res. Bull.*, 2003, **38,** 41-54.

42 P. An, F. Zuo, Y. P. Wu, J. H. Zhang, Z. H. Zheng, X. B. Ding and Y. X. Peng, *Chin. Chem. Lett.*, 2012, **23,** 1099-1102.

View Article Online
DOI: 10.1039/C5RA09114D

43 Y. J. Xie, B. Yan, H. L. Xu, J. Chen, Q. X. Liu, Y. H. Deng and H. B. Zeng, *Appl. Mater. Interfaces*, 2014, **6,** 8845-8852.

44 A. J. Ma, Y. J. Xie, J. Xu, H. B. Zeng and H. L. Xu, *Chem. Commun.*, 2015, **51,** 1469-1471.

45 H. L. Zhang, X. C. Li, G. H. He, J. J. Zhan and D. Liu, *Ind. Eng. Chem. Res.*, 2013, **52,** 16902-16910.

46 J. Z. Jiang, J. Zou, L. H. Zhu, L. Huang, H. P. Jiang and Y. X. Zhang, *J. Nanosci. Nanotechno.*, 2011, **11,** 4793-4799.

47 J. Hu, Y. L. Dong, Z. U. Rahman, Y. H. Ma, C. L. Ren and X. G. Chen, *Chem. Eng. J.*, 2014, **221,** 16-24.

48 H. T. Wang, Z. X. Dong and C. Z. Na, *Sustainable Chem. Eng.*, 2013, **1,** 746-752.

49 H. Wang and Y. M. Huang, *J. Hazard. Mater.*, 2011, **191,** 163-169.

50 Z. Zhang, J. H. Hao, W. S. Yang, B. P. Lu, X. Ke, B. L. Zhang and J. L. Tang, *Appl. Mater. Interfaces*, 2013, **5,** 3809-3815.

51 A. Chithambararaj, N. S. Sanjini, A. C. Bose and S. Velmathi, *Catal. Sci. Technol.*, 2013, **3,** 1405-1414.

52 Q. Wang, S. L. Tian and P. Ning, *Ind. Eng. Chem. Res.*, 2014, **53,** 643-649.

53 Q. Wang, S. L. Tian, J. Long and P. Ning, *Catalysis Today*, 2014, **224,** 41-48.

54 Y. X. Wang, S. H. Wang, H. Y. Niu, Y. R. Ma, T. Zeng, Y. Q. Cai and Z. Meng, *J. Chromatogr. A*, 2013, **1283,** 20-26.

55 T. Hirakawa and Y. Nosaka, *Langmuir,* 2002, **18,** 3247-3254.

56 L. Su, J. Feng, X. M. Zhou, C. L. Ren, H. H. Li and X. G. Chen, *Anal. Chem.*, 2012, **84,** 5753-5758.

View Article Online
DOI: 10.1039/C5RA09114D

Figure captions:

Fig. 1. Schematic diagram of the synthetic strategy and application of $CuFe_2O_4$@PDA magnetic nanoparticles.

Fig. 2. TEM images of $CuFe_2O_4$ MNPs (a) and $CuFe_2O_4$@PDA MNPs (b).

Fig. 3. TEM images of the $CuFe_2O_4$@PDA MNPs based on $CuFe_2O_4$ sub-microspheres with different shell thicknesses: 15 nm (a), 24 nm (b), 32 nm (c), 55 nm (d) and 95 nm (e), corresponding to 0.5, 1, 2, 3, 4 mg mL^{-1} of DA monomer concentration, respectively. The EDX pattern of the $CuFe_2O_4$@PDA MNPs (f).

Fig. 4. FT-IR spectra of the $CuFe_2O_4$ MNPs (a) and $CuFe_2O_4$@PDA core-shell MNPs (b), respectively.

Fig. 5. Room-temperature magnetization hysteresis loops of the $CuFe_2O_4$ MNPs (a) and $CuFe_2O_4$@PDA MNPs (b).

Fig. 6. (a) UV-Vis absorption spectrum of MB degradation before and after addition of H_2O_2 and $CuFe_2O_4$@PDA MNPs. (b) Photograph of the reduction of MB by H_2O_2 in the presence of $CuFe_2O_4$@PDA MNPs.

Fig. 7. (a) Time-dependent degradation efficiency of MB in systems of MB + H_2O_2, $CuFe_2O_4$@PDA + MB + H_2O_2 and $CuFe_2O_4$ + MB+ H_2O_2. (b) Time-dependent adsorption efficiency of MB in systems of $CuFe_2O_4$ + MB and $CuFe_2O_4$@PDA + MB.

Fig. 8. Effects of reaction conditions on MB degradation efficiency. (a) dopamine monomer concentration. (b) the $CuFe_2O_4$@PDA MNPs amount. (c) H_2O_2 concentration. (d) pH.

Fig. 9. The time-dependent UV-Vis absorption spectra change for the reduction

View Article Online
DOI: 10.1039/C5RA09114D

process of MB. The illustration shows the relationship between $\ln(A_t/A_0)$ and reaction time (t) for the MB reduction.

Fig. 10. Successive UV-vis spectra of MB solution (black curve) and resultant solution after degraded by $CuFe_2O_4$@PDA MNPs (red curve).

View Article Online
DOI: 10.1039/C5RA09114D

Schemes and figures:

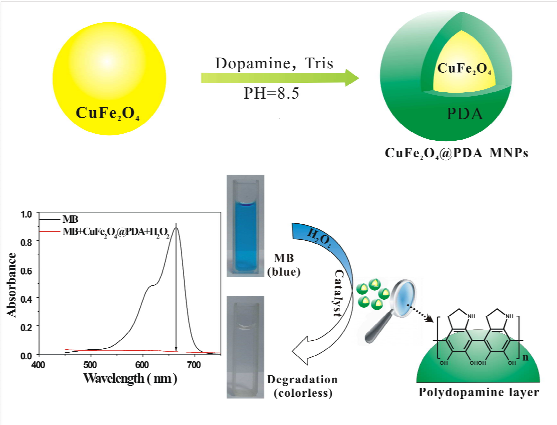

Fig. 1. Schematic diagram of the synthetic strategy and application of $CuFe_2O_4$@PDA magnetic nanoparticles.

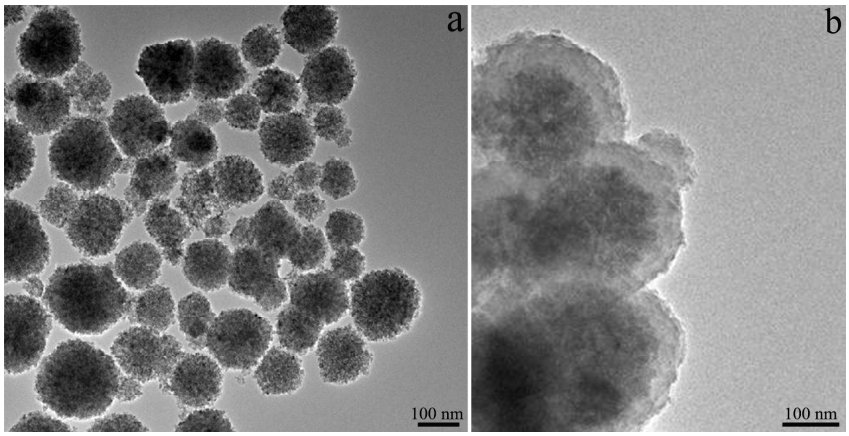

Fig. 2. TEM images of $CuFe_2O_4$ MNPs (a) and $CuFe_2O_4$@PDA MNPs (b).

View Article Online
DOI: 10.1039/C5RA09114D

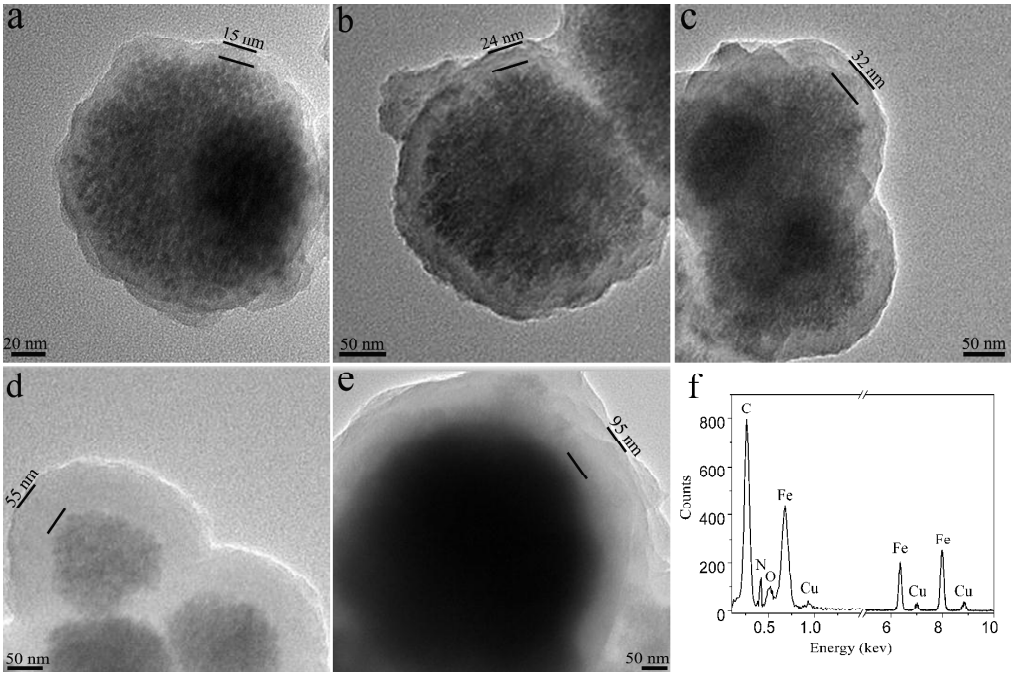

Fig. 3. TEM images of the $CuFe_2O_4$@PDA MNPs based on $CuFe_2O_4$ sub-microspheres with different shell thicknesses: 15 nm (a), 24 nm (b), 32 nm (c), 55 nm (d) and 95 nm (e), corresponding to 0.5, 1, 2, 3, 4 mg mL^{-1} of DA monomer concentration, respectively. The EDX pattern of the $CuFe_2O_4$@PDA MNPs (f).

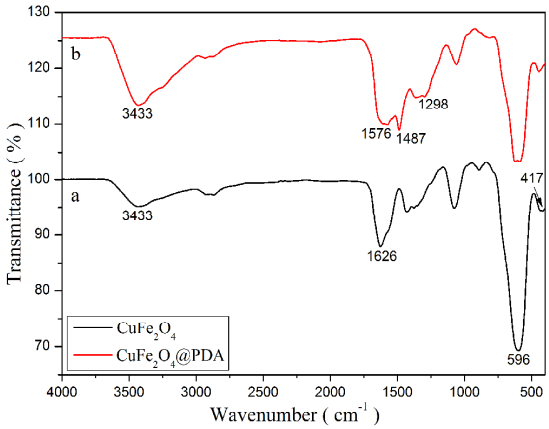

Fig. 4. FT-IR spectra of the $CuFe_2O_4$ MNPs (a) and $CuFe_2O_4$@PDA core-shell MNPs (b), respectively.

View Article Online
DOI: 10.1039/C5RA09114D

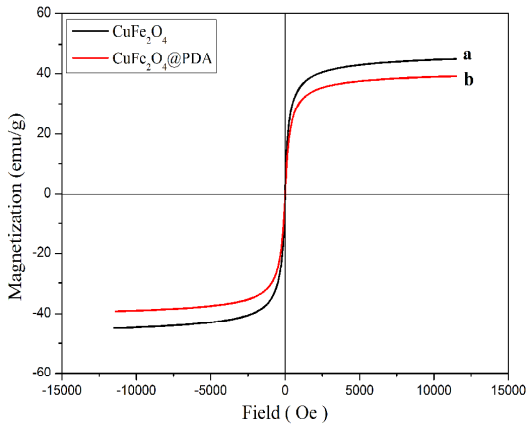

Fig. 5. Room-temperature magnetization hysteresis loops of the $CuFe_2O_4$ MNPs (a) and $CuFe_2O_4$@PDA MNPs (b).

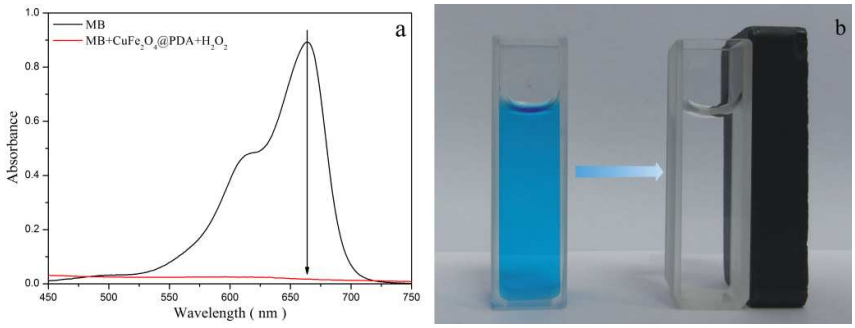

Fig. 6. (a) UV-Vis absorption spectrum of MB degradation before and after addition of H_2O_2 and $CuFe_2O_4$@PDA MNPs. (b) Photograph of the reduction of MB by H_2O_2 in the presence of $CuFe_2O_4$@PDA MNPs.

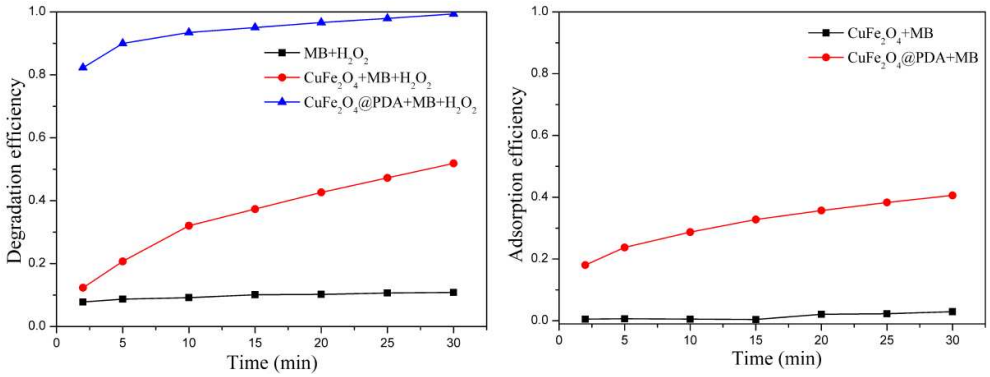

View Article Online
DOI: 10.1039/C5RA09114D

Fig. 7. (a) Time-dependent degradation efficiency of MB in systems of MB + H_2O_2, $CuFe_2O_4$@PDA + MB + H_2O_2 and $CuFe_2O_4$ + MB+ H_2O_2. (b) Time-dependent adsorption efficiency of MB in systems of $CuFe_2O_4$ + MB and $CuFe_2O_4$@PDA + MB.

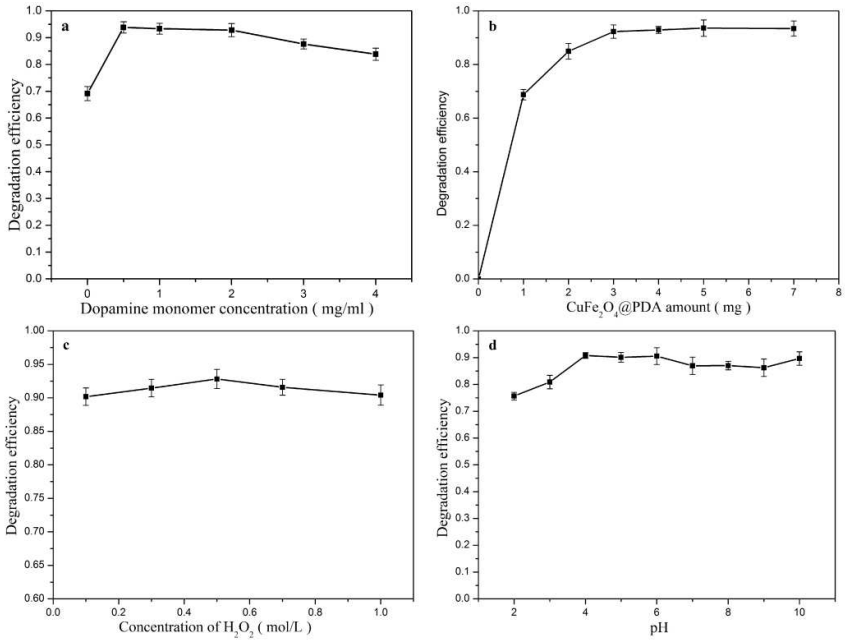

Fig. 8. Effects of reaction conditions on MB degradation efficiency. (a) dopamine monomer concentration. (b) the $CuFe_2O_4$@PDA MNPs amount. (c) H_2O_2 concentration. (d) pH.

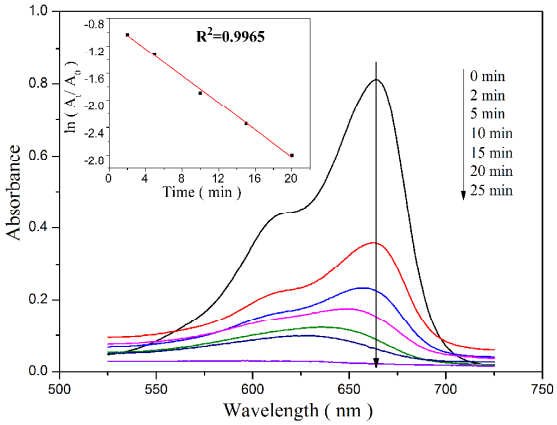

View Article Online
DOI: 10.1039/C5RA09114D

Fig. 9. The time-dependent UV-Vis absorption spectra change for the reduction process of MB. The illustration shows the relationship between $\ln(A_t/A_0)$ and reaction time (t) for the MB reduction.

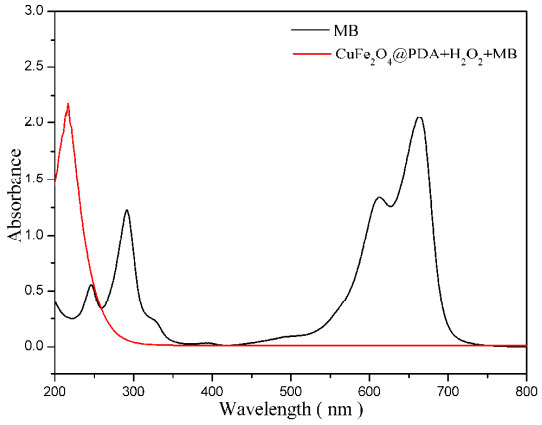

Fig. 10. Successive UV-vis spectra of MB solution (black curve) and resultant solution after degraded by $CuFe_2O_4$@PDA MNPs (red curve).